J Appl Electrochem (2014) 44:263–277
DOI 10.1007/s10800-013-0654-y

RESEARCH ARTICLE

Modification of well-aligned carbon nanotubes with dihexadecyl hydrogen phosphate: application to highly sensitive nanomolar detection of simvastatin

H. Fayazfar · A. Afshar · A. Dolati · M. Ghalkhani

Received: 5 August 2013 / Accepted: 2 December 2013 / Published online: 10 December 2013

Abstract The first usage of dihexadecyl hydrogen phosphate (DHP)-modified highly oriented multi-walled carbon nanotube (MWCNTs) forests in a sensor configuration was developed to investigate the electrochemical oxidation and determination of simvastatin (SV) in pharmaceutical dosage forms. Synthesis of well-aligned MWCNTs on a conductive Ta substrate by catalytic vapor deposition technique using a common chemical, ethylenediamine, and without being plasma-aided was reported. The electrochemical behavior and oxidation of SV at the aligned MWCNTs/DHP/Ta electrode were discussed in detail through cyclic voltammetry and differential pulse voltammetry. This modified electrode showed considerably higher electrocatalytic activity for SV than bare Ta electrode or entangled MWCNTs powder electrode, due to presence of the alignment and mutual separation of CNTs. Under the optimal conditions, the A-MWCNTs/DHP/Ta-modified electrode showed a wide linear range from 0.01 to 1 μM with a detection limit of 0.01 nM demonstrating promising results for the future usage in clinical applications.

Keywords Voltammetry · Electrochemical oxidation · Simvastatin · Sensors · Multi-walled carbon nanotube

H. Fayazfar · A. Afshar · A. Dolati (✉)
Materials Science and Engineering Department, Sharif University of Technology, P.O. BOX 11155-9466, Tehran, Iran
e-mail: dolati@sharif.edu

H. Fayazfar
e-mail: r.fayazfar@gmail.com

M. Ghalkhani
Department of Chemistry, Faculty of Science, Shahid Rajaee Teacher Training University, Lavizan, Tehran, Iran

1 Introduction

Cholesterol is an important lipid found in cells and membranes of all animal tissues. However, high cholesterol accumulation in the blood serum is strongly correlated with diseases such as coronary heart disease, arteriosclerosis, and brain thrombosis [1, 2]. Simvastatin (SV), an inactive lactone, is hydrolyzed in vivo to the corresponding β,δ-dihydroxyl acid (simvastatin acid, SVA) after oral administration [3]. The latter is a potent inhibitor of HMGCoA and can effectively reduce the content of low-density lipoprotein cholesterol in plasma [3]. Therefore, the estimation of SV quantity is of interest to both the biologic science and food industries [2]. A variety of analytical procedures for SV detection have been proposed. Although these techniques were sensitive and selective, they usually suffered from some inevitable disadvantages; hence, it is desired to develop techniques for cost-effective, convenient, rapid, and sensitive estimation of SV [4–7]. In recent years, electrochemical sensors employing chemically modified electrodes have become interesting because of their good performances such as high sensitivity and good selectivity [7, 8]. Various nanomaterials are employed to fabricate modified electrodes which among them, carbon nanotubes (CNTs) have been widely used to improve the sensitivity in detecting some drugs. CNTs have been paid much of attention since their discovery in 1991 [9–11], due to their unusual structures and unique properties [16]. Moreover, CNTs, when used as electrode materials in electrochemical reactions, have shown an outstanding ability to mediate fast electron transfer kinetics for important biomolecules [12–14]. Well-aligned and mutually separated CNTs which possess regular pore structures, conductive paths, and high specific surface areas offer distinct advantages in comparison with loose and randomly

oriented CNT powders that often need assembly or integration [15, 16]. Compared with indirectly connecting the aligned CNTs (A-CNTs) to the current collectors (transfer techniques) [17], growing A-CNTs directly on conductive substrates is more attractive due to high-quality CNT-metal contact and one-step process [18, 19]. The unique advantages of the direct growth of A-CNTs on Ta substrates will be that first individual nanotubes are electrically connected with the conductive acid-resisting substrates and second this promoted electron transfer is thus leading to excellent overall sensing characteristics which overcome several obstacles to applications in chemical and biologic sensing [17, 19, 20]. In addition, based on the hydrophobic interactions between the hydrophobic tails of dihexadecyl hydrogen phosphate (DHP)—a water insoluble surfactant—and the sidewall of the nanotubes as well as the possible interactions between the phosphate groups on DHP and the oxygen-containing groups on acid-treated CNTs, in this study an efficient way to introduce DHP onto well-aligned CNTs for adsorbing SV was used.

In the present study, on the basis of the enhanced oxidation of SV at well-aligned multi-walled carbon nanotube/DHP-modified Ta electrode (A-MWCNTs/DHP/TaE), an effective electrochemical method for the determination of SV was developed. A field emission scanning electron microscope (FESEM) and a transmission electron microscope (TEM) were used to observe the morphology, alignment, and nanostructures of the prepared A-MWCNTs. Cyclic voltammetry (CV) and differential pulse voltammetry (DPV) were used to investigate the electrocatalytic activity of electrodes toward SV oxidation.

2 Experimental

2.1 Chemicals and instrumentation

SV, L-ascorbic acid (AA), uric acid (UA), $NiCl_2{\cdot}6H_2O$ (99.99 %), and DHP were purchased from a commercial vendor (Sigma-Aldrich). All other reagents were of analytical grade and used without further purification. All solutions were freshly prepared daily with high-quality deionized water. FESEM (MIRA TESCAN operating at 20 kV) was used to observe the morphology and nanostructures of the prepared A-MWCNTs. TEM measurements were performed with a Philips EM 208 FEG instrument operating at 90 kV. The surface chemistry of the as-grown CNTs and the electrochemically modified CNT arrays with oxygen-containing groups (functional groups) were confirmed by fourier transformed infrared (FTIR) and Raman investigations. Raman spectrum was measured on a micro-Raman spectrometer (an Almega Thermo Nicolet Dispersive Raman Spectrometer, a Nd:YLF laser emitting at 532 nm, was used for excitation. Spectral resolution of the spectrometer was 4 cm^{-1}). The FTIR spectra were obtained with a Perkin Elmer PC16 FTIR instrument using the attenuated total reflection technique. The nitrogen content and the stability of the nitrogen incorporated in nitrogen-doped carbon nanotubes (CNx) were studied by Kratos Axis Ultra Al (alpha) X-ray photoelectron spectroscopy (XPS) operated at 14 kV. Electrochemical measurements were performed with a potentiostat–galvanostat AutoLab electrochemical analysis system supplied with a FRA 2.0 module (Echo Chemie BV Model PGSTAT-302 N, Netherlands). A three-electrode system was employed for electrochemical oxidation of SV with bare or A-MWCNTs/DHP-modified Ta substrate as working electrode (surface area is 0.3 cm^2), a saturated calomel reference electrode (SCE), and a platinum wire counter electrode. All potentials were quoted versus this reference electrode, and the measurement was performed at room temperature (25 °C). Electrochemical impedance spectroscopy (EIS) was also performed in a solution containing 5.0 mM $K_3[Fe(CN)_6]/K_4[Fe(CN)_6]$ and 0.10 M KCl. The EIS measurements were recorded within the frequency range of 1 mHz to 10 kHz at a potential of 0.17 V and a voltage amplitude of 5 mV. CV studies were performed in phosphate buffer solution (PBS) (0.1 M, pH = 4) at a scan rate of 20 mV s^{-1}.

2.2 Procedures

2.2.1 Synthesis of well-aligned MWCNTs

Well-aligned MWCNTs were synthesized on small Ta plates by CVD with ethylenediamine as a precursor in which the amine serves as both an etching reagent for the formation of catalytic metal nanoparticles and a carbon source for the growth of A-MWCNTs. The Ta plate substrate is an ideal one, because it is chemically inert, highly conductive, and relatively inexpensive, with a high melting point enabling it to endure high temperature, which is required for growing MWCNTs. At first, Ta substrates were polished until a mirror-like surface was created and then were ultrasonically cleaned in ethanol before MWCNT growth. The 0.01–1 M ethanol solution of metal salt $NiCl_2{\cdot}6H_2O$ has been prepared in an argon (Ar)-filled glovebox. After that, Ta substrate was coated (sprayed) with drops of metal chloride solution and was dried by Ar. In some samples after drying by Ar, the substrate was sprayed with metal chloride solution for the second time to create two layers of catalyst on the Ta and then was dried by Ar (in order to increase the catalyst thickness). The Ni-coated Ta plates were directly put into the middle of the quartz tube reactor that was preheated to 850 °C. The substrates were pretreated by N_2 with a flow rate of

500 sccm for 5–20 min, forming the nano-sized catalytic particles. After purging and preheating with N_2, the ethylenediamine was introduced by bubbling N_2 at a flow rate of 500 sccm through liquid ethylenediamine contained in a glass bottle. Thus, the formed feeding gas contained approximately 8 % ethylenediamine. The reaction times were varied from 5 to 45 min, after which the reactor was cooled down to room temperature in N_2 ambient. By altering the growth time and catalyst thickness, well-aligned MWCNTs with uniform size, good distribution, and high density were produced. The dimensions of the MWCNTs are 20–100 nm in diameter and several microns in length. To electrochemically purify CNTs with keeping their alignment and introducing functional groups to them, the MWCNTs electrode was immersed in 0.2 M HNO_3 solution, and the potential was cycled between +1.00 and +2.00 V at a scan rate of 50 mV s^{-1}. For the preparation of A-MWCNTs/DHP/TaE, 3.0 mg DHP was added to 4.0 mL water and briefly sonicated in water bath for 30 min; then DHP-modified electrode was prepared by applying DHP onto the A-MWCNTs/DHP/Ta substrate using a micropipette and allowing them to dry at room temperature. The A-MWCNTs/DHP/TaE was completely rinsed with ultrapure water to remove the unabsorbed DHP, and then it was dried in air at room temperature.

2.2.2 *Investigation of SV oxidation at the A-MWCNT/DHP/Ta electrodes*

CV and DPV were used to investigate the electrocatalytic activity of electrodes toward SV oxidation. The stock solution of SV (1.0 mM) was prepared by dissolving SV into absolute ethanol and then diluted to working solutions with various concentrations of the supporting electrolyte. A PBS (0.1 M) was placed into an electrochemical cell as the supporting electrolyte, and different amounts of SV were added. DPV employed a potential range of 0–1.5 V, pulse amplitude of 50 mV, pulse period of 0.2 s, and pulse width of 50 ms. For comparison, the electrochemical oxidation of SV at bare Ta electrode and entangled MWCNTs powder was also investigated. Every single measurement was repeated three times using similar electrodes.

3 Results and discussion

3.1 Synthesis and characterization of the well-aligned MWCNTs on the Ta substrate

Figure 1a, b shows SEM images of the grown well-aligned CNTs on the polished Ta substrate at 850 °C after 6 min. As it can be seen, well-aligned CNTs can grow on the substrate surface with proper orientation and density. Regarding investigation of the different parameters on the CNTs growth and alignment, it was observed that well-aligned CNTs with diameter between 20 and 100 nm and length of several micrometers were produced using chloride-nickel solution on the polished substrate (with concentration of 0.1 M), preheating the substrate for 4 min to produce the metallic nanoparticles and then allowing CNTs to grow at 850 °C after 6 min. Figure 1c, d also shows TEM images of the vertically A-CNTs. In Fig. 1c, it can be seen that CNTs have bamboo-like structures and achieved CNTs are multi-layered. Also, in the Fig. 1d, it can be observed that tips of the CNTs are closed. No catalyst particle can be observed on the tip of the CNTs, indicating that root growth was dominant in which catalyst particles are kept stuck onto the substrate surface.

3.2 Purification of well-aligned A-MWCNTs on the Ta substrate by electrochemical oxidation and their characterization

Electrochemical oxidation of A-CNTs was performed using CV at the potential between 1 and 2 V and scan rate of 50 mV/s in nitric acid with concentration of 0.2 M. Then, CNTs were washed with deionized water and dried in the oven with temperature of 80–100 °C to keep their alignment and orientation. This implies that drying the CNTs in ambient temperature makes them to be curved, clustered, severely agglomerated, and damaged in terms of alignment. Such agglomeration and collapse are highly undesirable as a major portion of the CNT surface is now blocked and less accessible for electrochemical reactions. Therefore, adhesion forces should be omitted or lowered during evaporation to stop CNTs agglomeration [21]. To avoid CNT agglomeration and collapse caused by the liquid–gas interface, a simple oven-drying step was introduced after the electrochemical oxidation of CNTs to eliminate the surface tension force during the evaporation of the water.

To characterize chemical groups on CNTs surface, FTIR and Raman spectra of vertically A-CNTs before and after electrochemical oxidation in nitric acid were measured and analyzed. Figure 2 shows FTIR spectra of CNTs before and after electrochemical oxidation in nitric acid. It can be observed that very weak peaks appear in Fig. 2a and the spectrum of the as-prepared MWCNTs shows the C–C stretching bonds in the range of 1,580–1,650 cm^{-1} characteristic to the expected nanotube phonon modes. The absorption band related to C–N bond can be observed at 1,110 cm^{-1} which indicates the appearance of nitrogen groups upon using ethylendiamine in a N_2 flow in CVD process [22]. The HNO_3 oxidative treatment produces oxygen-containing groups on the surface of the MWCNTs (Fig. 2b). It can be seen that the peak in 1,715 cm^{-1} is

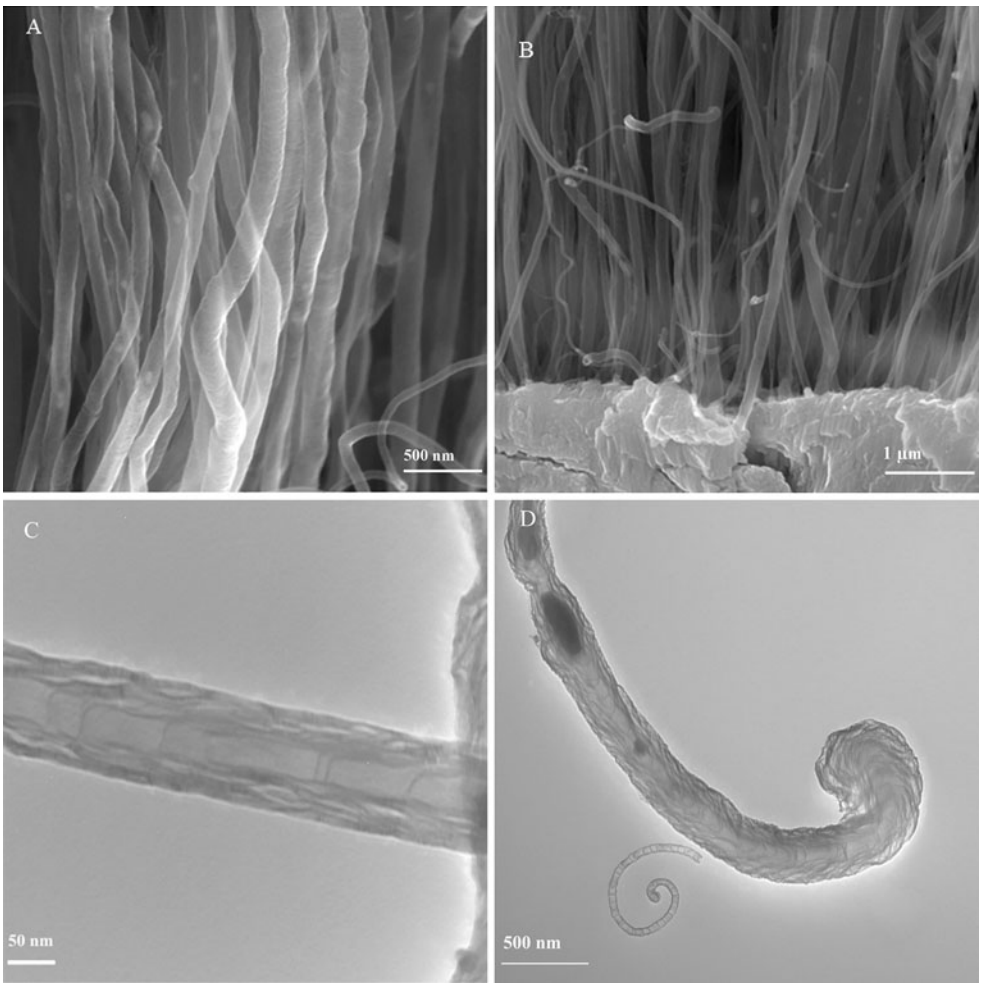

Fig. 1 **a**, **b** SEM images of well-aligned CNTs grown on the polished Ta substrate at 850 °C after 6 min shown with different resolutions. **c**, **d** TEM images of Bamboo-like structure multi-walled CNTs

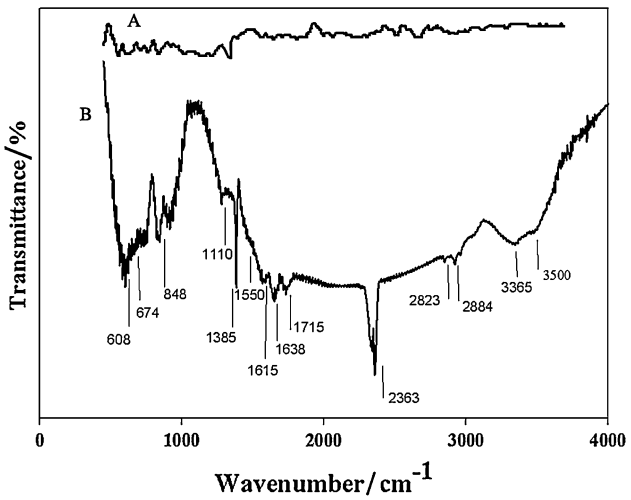

Fig. 2 **a** FTIR spectrum of CNTs before and **b** after electrochemical oxidation in nitric acid

associated with –C=O stretching of the carboxyl group. Peaks around 3,000–3,500 cm^{-1} are associated with –O–H stretching bond in carboxyl and hydroxyl groups. The absorption band related to C–N bond can be observed at 1,110 cm^{-1} which indicates the appearance of new amine functional groups upon functionalization process in HNO_3. Peaks occurred in 2,884 and 2,823 cm^{-1} are associated with C–H stretching bond in aliphatic $–CH_2$ and CH_3 groups. Deformation and bending of different types of C–H bonds are characterized by peaks below 900 cm^{-1} [23, 24]. In fact, bands in the range of 1,750–1,550 cm^{-1} can be associated to C=O groups, in different environments (carboxylic acid, ketone/quinone), and to C=C in aromatic rings; while bands in the range of 1,300–950 cm^{-1} prove the presence of the C–O bonds in various chemical surroundings. C=O bonds as characteristics of carboxyl functional groups (–COOH) and ketone/quinone can be observed in 1,711 and 1,638 cm^{-1} [25, 26].Observed peak

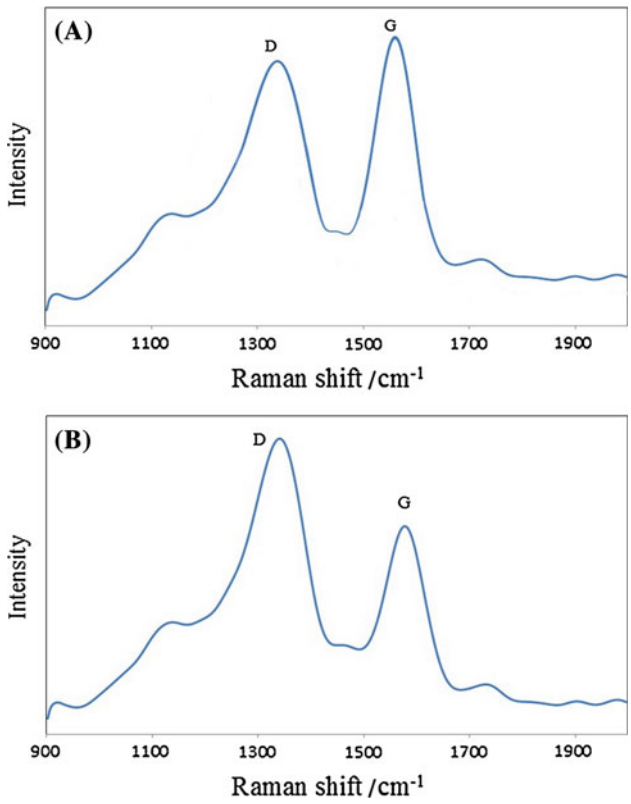

Fig. 3 **a** Raman spectra of CNTs before and **b** after electrochemical oxidation in nitric acid, with different D-band and G-band modes

around 2,363 cm^{-1} also can be associated to ionic amines $C{=}NH^{+}$.

Raman spectrometry is a beneficial tool in analyzing degree of graphitization of carbon-based materials. Figure 3 shows Raman spectra of the CNTs before and after electrochemical oxidation in nitric acid. Observed Raman band in 1,584 cm^{-1} is attributed to the stacking of the graphite hexagon network plane (G-band), while the other band in 1,347 cm^{-1} is related to the amorphous carbon or deformation vibrations of a hexagonal ring (D-band) [27, 28]. Since G-band modes depend on diameter, it is clear that G-band occurred for CNTs with big diameters would be similar to that of graphite single peak G-band. This similarity can be seen for MWCNTs where a single peak occurs around 1,584 cm^{-1} which is like that of graphite. However, in SWNT, this band has two peaks which uniquely belonged to single-walled CNTs. Therefore, it can be concluded that obtained CNTs in this research are multi-walled CNTs. It is acknowledged that the ratio of the intensities of the D and G peaks (I_D/I_G) reveals useful information on the graphitization degree and lattice distortion of the carbon-based materials [29]. The D-band indicates, as usual for carbon nanostructures, the density of defects and can be used for monitoring the process of functionalization which transforms sp^2 to sp sites. Different I_D/I_G ratios of the samples illustrate different crystalline structures. The as-synthesized A-CNTs have the I_D/I_G ratio of 0.91 before electrochemical oxidation, while this ratio was equal to 1.48 for functionalized CNTs. This increase can be attributed to the electrochemical oxidation. Furthermore, a considerable shift in G mode (+14 cm^{-1}) can be seen which is related to the changes in MWCNTs electrochemical structure due to the change in amount and type of the chemical groups attached to the walls and tips of the A-CNTs and/or amount of the increased oxygen content in CNTs structure that can act as p-type dopant [30].

To obtain more information on the relationship of nitrogen concentration in the CNx tubes, XPS analysis was carried out. The full-range XPS spectra of CNx tubes are exhibited in Fig. 4a. We obtained four main peaks at 285, 401, 531, and 850 eV. They are attributed to C 1*s*, N 1*s*, O 1*s*, and Ni 2*p* signal, respectively. The strong C peak can be assigned to sp^2-hybridized carbon, which is the major component in CNx tubes. The nitrogen content of each sample has been calculated and listed in Table 1. The N 1*s* spectrum and related nitrogen profile are demonstrated in Fig. 4b, c. The symmetric N 1*s* spectra indicate the existence of several components. The spectra are fitted into four to five peaks. The peaks around 399.0–400.1 and 401.5–402.4 eV are attributed to pyridine-like nitrogen and graphite-like nitrogen [31]. Pyridine-like atoms contribute to the π system with a pair of π electrons and bonding to two carbon atoms. While, the graphite-like nitrogen corresponds to highly coordinated nitrogen atoms substituting inner carbon atoms on the graphite layers. The peaks around 403.1–403.8 eV are assigned to oxidized nitrogen which is bonded with oxygen. The peaks around 405.3–406.1 eV are ascribed to the nitrogen atoms that form endohedral or exohedral complex with carbon–carbon bond on the tube walls [31], which are called sorbed nitrogen. It has also been proved that these nitrogen atoms are covalently bound to the carbon nanotubes [32]. The highest bonding energy band arise at around 407.8–408.9 eV can be attributed to molecular nitrogen, because previous reports show molecular nitrogen can be encapsulated inside the tubes [33] or exist as intercalated form between graphite layers during the formation of CNx tubes [34]. The nitrogen species stability in an acid environment is also studied. In this electrochemical acid treatment, the Ni signals were almost negligible after acid treatment indicating removal of the residual Ni catalyst (Table 1; Fig. 4a). The nitrogen content slightly increases after acid treatment. This is because the carbon impurities such as graphite nanoparticles and amorphous carbons can be eliminated after washing with acid [35]. The molecular nitrogen was released after acid treatment because of its weak bonding to graphite layers. The intensity of graphite-

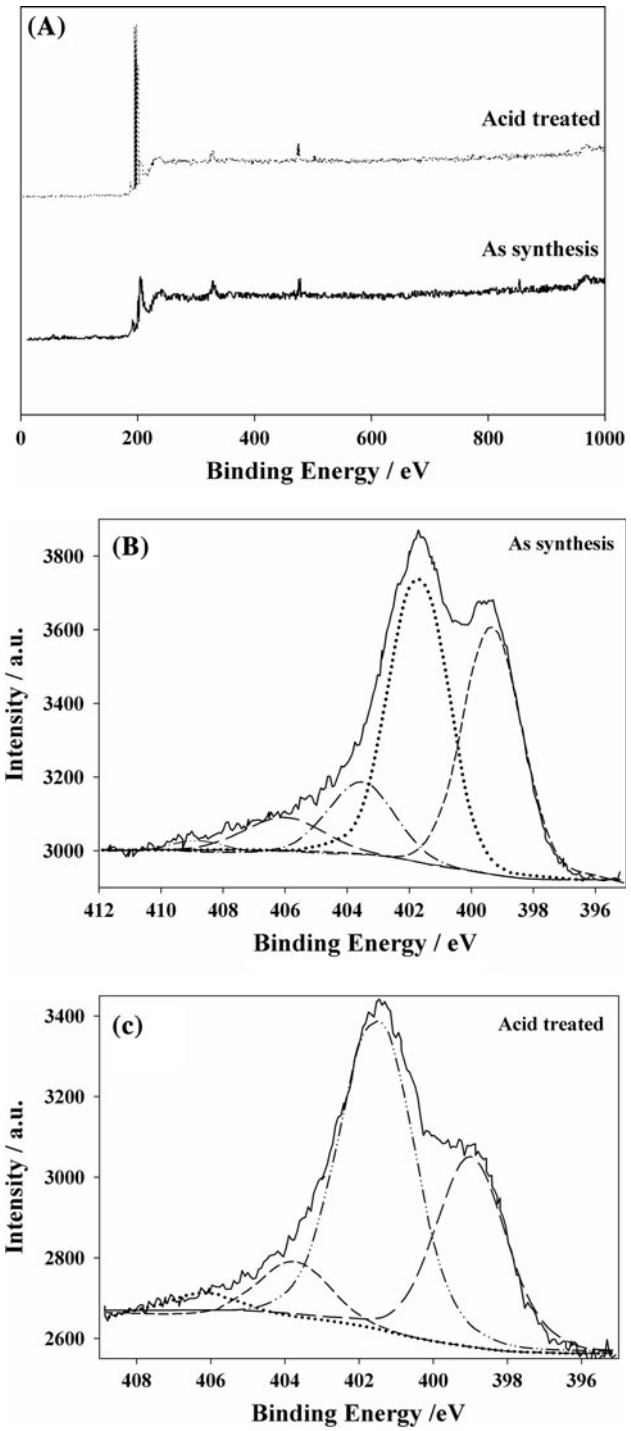

Fig. 4 XPS spectrum of the nitrogen-doped MWCNTs **a** in full range and N 1*s* XPS spectrum of the CNx tubes **b** as-synthesized, **c** after acid treatment

like nitrogen increases, because graphite-like nitrogen has a higher bonding energy and graphite-like nitrogen atoms are located in inner graphene layers, which is hard for acid to achieve. On the other hand, pyridine-like nitrogen prefers to exist at the open edges of the bamboo kink to stop its growth [36], then it is easier for acid to react with pyridine-like nitrogen atoms.

3.3 Electrochemical behavior of the A-MWCNTs/DHP/TaE in PBS solution

Typical voltammetric responses of bare TaE and A-MWCNTs/DHP/TaE in PBS (pH = 4.0) are shown in Fig. 5. No oxidation peaks were observed in the absence of SV for both electrodes. The bare TaE gave a very small current response (Fig. 5a). However, when A-MWCNTs/DHP/TaE was used, the background current is significantly enhanced (Fig. 5b). This result implies that CNTs exhibit very high specific capacitances which are resulted of the high accessible nanotube surface area in electrolyte that make it appropriate for electrochemical devices.

EIS was employed to investigate the impedance changes of the electrode surface due to the modification procedure. Figure 6 shows the Nyquist plots of $K_3Fe(CN)_6/K_4Fe(CN)_6$ at the bare Ta and the A-MWCNT/TaE. In these studies, high frequency zone, which appears as a semicircle plot, can be ascribed to the kinetic limitations (R_{ct}) of the electrochemical reaction. On the other hand, the linear behavior of Z_{Im} versus Z_{Re} in a low frequency region is characteristic of a diffusion-controlled electrode process. As can be seen in Fig. 6a, a semicircle with a very large diameter is observed at the bare TaE. However, the diameter of the semicircle is significantly reduced with A-MWCNT/TaE, which suggests that the surface of the modified electrode exhibits lower electron transfer resistance and greatly increases the electron transfer rate (Fig. 6b). In fact, binding of A-MWCNTs on the electrode surface generated a conducting porous layer on the electrode surface that functioned as a promoter to the interfacial electron transfer. Also, it is interesting that the R_{ct} values for nitrogen-doped MWCNT-modified electrode are somewhat smaller compared to those obtained on film consisting of pristine MWCNTs (Fig. 10). The last finding confirms the important effect of nitrogen doping on electrocatalytic activity of carbon nanotubes, which has been explained in detail in Sect 3.4.

A-MWCNT/DHP/TaE denotes the nitrogen-doped-modified electrode for all investigations.

3.4 Voltammetric behavior of SV

The electrochemical responses of 1.0 μM SV in PBS (0.1 M, pH = 4.0) at different electrodes were investigated (Fig. 7). Figure 3a shows the cyclic voltammograms of SV at bare Ta substrate. When the electrode potential scans from 0.5 to 1.5 V, a small oxidation peak ($i_p = 25$ μA cm^{-2}) at 1.31 V is observed. On the scan reversal, no reduction peak appears, indicating the

Table 1 Ni catalyst content, nitrogen content, and related detailed nitrogen distribution of CNx tubes

Treating conditions	Nitrogen content (%)	Pyridine-like nitrogen (%)	Graphite-like nitrogen (%)	NO_x (%)	Sorbed nitrogen (%)	Molecular nitrogen (%)	Ni (%)
As-synthesized	7.6	35.1	42.7	14.1	6.9	1.2	2.35
Acid-treated	8.9	28.3	56.6	11.3	3.7	–	0.11

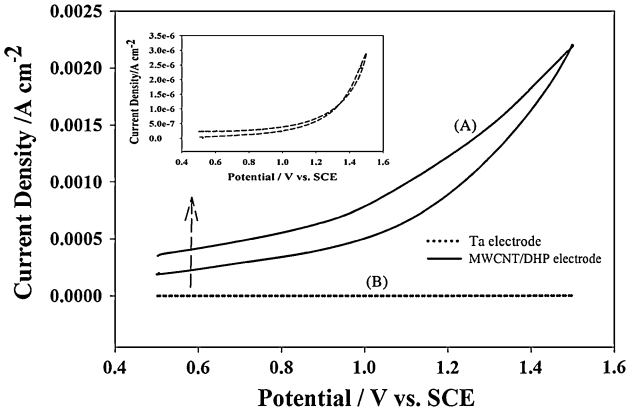

Fig. 5 Cyclic voltammograms of **a** the A-MWCNTs/DHP/Ta electrode, **b** the Ta electrode in PBS (pH = 4). Scan rate = 20 mV s^{-1}

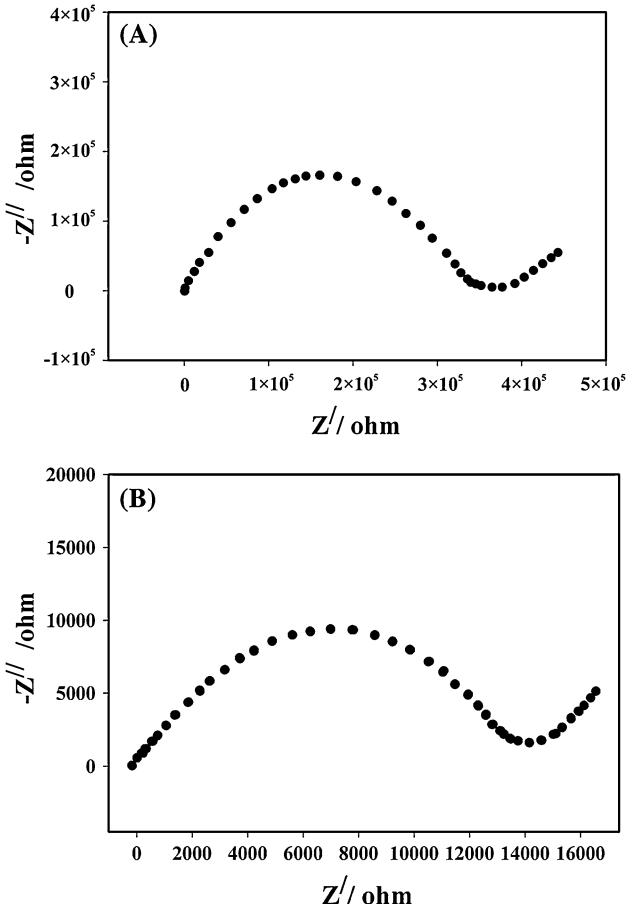

Fig. 6 Nyquist diagram (Z'' vs. Z') for the EIS measurements in 5 mM $K_3Fe(CN)_6/K_4Fe(CN)_6$ + 0.1 M KCl for the bare Ta (**a**) and the A-MWCNT/TaE (**b**)

completely irreversible oxidation of SV. At the DHP/TaE, the oxidation peak of SV completely disappears, and the background current apparently decreases (Fig. 7b). The modification of surface of TaE with DHP might result in the formation of a compact hydrophobic and insulate layer of DHP at the electrode surface, which not only decreases the conductivity of the electrode, but also blocks the mass transfer of SV. At the A-MWCNT/DHP/TaE, the obvious oxidation peak of SV at 1.2 V appears, with an increase in peak current as compared to that of Ta electrode (Fig. 7c). Compared with the poor responses at bare TaE, the oxidation of SV at the A-MWCNT/DHP/TaE is significantly improved, reflected by the greatly enlarged peak current (i_p = 0.0044 A cm^{-2}) and the negative shift of the peak potential (E_p = 1.2 V) (Fig. 7c). The decrease in the anodic overpotential for SV shows a strong catalytic function of the A-MWCNTs toward the oxidation of SV. The shifts in the overpotential may be due to a kinetic effect by which an increase in the rate of electron transfer from SV to the A-MWCNT/DHP/TaE can be attributed to improved electron transfer processes on the A-MWCNT/DHP/TaE. Also, Fig. 7d shows the cyclic voltammograms of SV at DHP-modified random-distributed MWCNTs powder. It can be seen that the response current to 1.0 μM SV is 0.0003 A cm^{-2}, which is over 14-fold lower than the well-aligned MWCNT/DHP/TaE value (0.0044 A cm^{-2}).

So, well-aligned but mutually separated MWCNTs offer distinct advantages over loose and randomly oriented CNT powders to effectively increase electrocatalytic activity, because they have high surface area which can promote electron transfer due to their regular porous structure and conductive paths. In addition, the cyclic area is also enlarged significantly at the A-MWCNT/DHP/TaE compared to the bare TaE, DHP/TaE, and DHP-modified MWCNTs powder. The enlarged cyclic area may originate from the large surface area created by the presence of A-MWCNTs as a double layer capacitance [37]. Therefore, the current electrode acts as a supercapacitor to enhance the electrochemical reaction and increase the rate of the heterogeneous electron transfer; thus, it obviously increased current response toward the oxidation of SV in

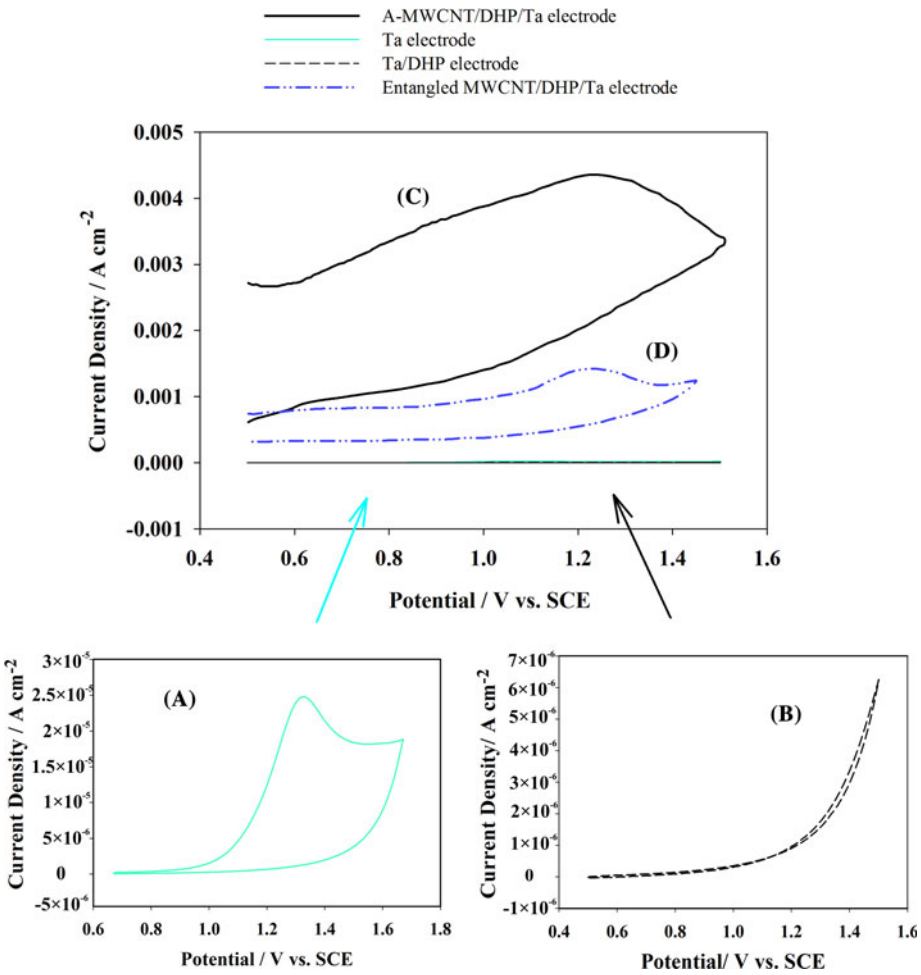

Fig. 7 Cyclic voltammograms of 1×10^{-6} M SV in 0.1 M PBS at: **a** Ta electrode; **b** Ta/DHP electrode; **c** A-MWCNT/DHP/Ta electrode; **d** entangled MWCNT/DHP/Ta electrode. Scan rate = 20 mV s^{-1}

contrast to the other electrodes. In fact, there were some MWCNTs spanning across the insulate DHP layer which might provide some active sites for the electrochemical reactions of biomolecules. Obviously, mentioned improvements confirm the ability of prepared A-MWCNT/DHP/TaE for detection of SV in PBS solution. In addition, the DHP layer might also be essential to the sensitive oxidation of SV at the MWCNT/DHP/TaE since hydrophobic SV might be adsorbed on the hydrophobic surface of DHP layer and be accumulated. So, no oxidation peak was observed using MWCNT/TaE without DHP for SV detection (data not shown here). The role of the DHP layer in enhancing SV oxidation, is supported by the influence of accumulation conditions on oxidation current, is discussed in Sect. 3.8.

Figure 8 shows the successive cyclic voltammograms (3 cycles) for SV in PBS (0.1 M) at the A-MWCNT/DHP/TaE. Similar to Fig. 7c, a sensitive oxidation peak appears on the first cycle of CVs. However, this oxidation peak completely disappears on the second and the following cycles, due to the strong adsorption of the oxidized product. It is clear that the possible group on SV that could be

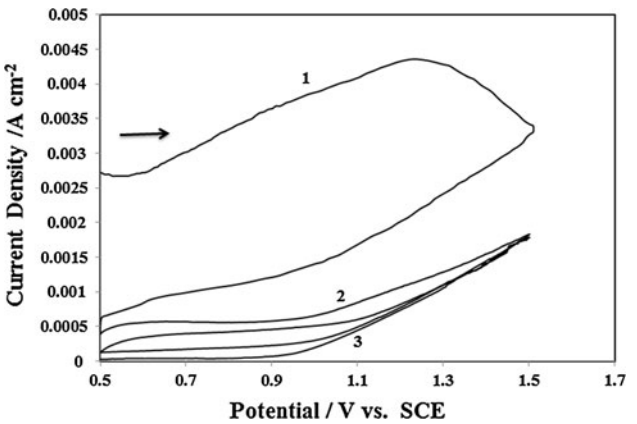

Fig. 8 Successive cyclic voltammograms (in three scans) of 1×10^{-6} M SV in PBS (0.1 M, pH = 4) at A-MWCNTs/DHP/Ta electrode. Scan rate = 20 mV s^{-1}. The numbers labeled were: (*1*) the first scan; (*2*) the second scan; (*3*) the third scan

oxidized is the β-hydroxyl group, since SV might exist in the lactone form in strong acidic media [38]. Absorption of SV on the hydrophobic DHP layer after oxidation leads to the formation of a compact film of the oxidized product and

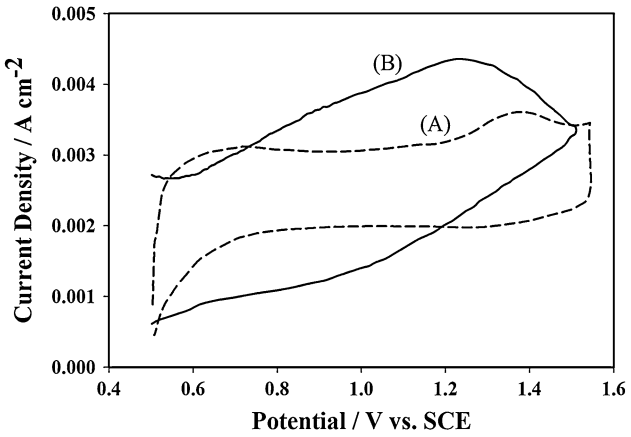

Fig. 9 Cyclic voltammograms of 1×10^{-6} M SV in 0.1 M PBS at: **a** p-MWCNT/DHP/TaE and **b** MWCNT/DHP/TaE; Scan rate = 20 mV s^{-1}

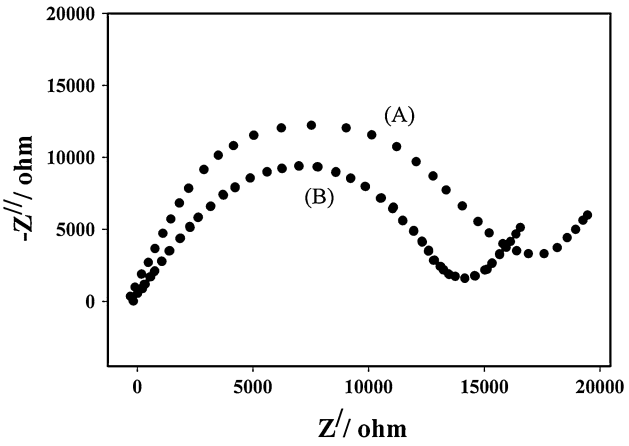

Fig. 10 Nyquist diagram (Z'' vs. Z') for the EIS measurements in 5 mM $K_3Fe(CN)_6/K_4Fe(CN)_6$ for the pristine MWCNT/TaE (**a**) and the nitrogen-doped A-MWCNT/TaE (**b**)

the sequential block of mass transfer of SV in solution at the A-MWCNT/DHP/TaE.

3.5 Effect of the nitrogen content at A-MWCNT/DHP/TaE on sensing performance

Nitrogen-doped carbon nanotubes have attracted particular research interest because of their applications in producing different types of nanodevices with tuning properties. Previous reports have indicated that controlled nitrogen doping can modulate the morphology, improve the reactivity, and enhance the field emission of the pristine carbon nanotubes. Doped nitrogen atoms mainly exist in two forms, substitutional and pyridinic nitrogen (also called graphite-like and pyridine-like nitrogen), both are chemically active for improving the surface reactivity of CNTs because of the presence of electron donor [39]. On the other hand, doping CNTs with N to yield a large number of defective sites onto the nanotube surfaces is proven to be an efficient method to regulate the structural and electronic properties of the nanotubes. Also, it is well-known that the nitrogen doping has an important effect on the electrochemical properties of MWCNTs. Namely, as was already reported in literature, the nitrogen-doped carbon nanotubes possess a marked electrocatalytic activity and improve the quality of electrochemical sensors [40, 41].

For investigation of the nitrogen effect on sensing performance, the typical cyclic voltammograms obtained at pristine MWCNTs (p-MWCNT/DHP/TaE) without nitrogen doping (A) and nitrogen-doped MWCNTs (MWCNT/DHP/TaE) electrode (B) in 0.10 M pH 4.0 PBS in the presence of 1×10^{-6} M SV (Fig. 9). A small peak at 1.4 V corresponding to the oxidation of SV was observed at p-MWCNT/DHP/TaE (Fig. 9a). On the other hand, nitrogen-doped MWCNT/DHP/TaE exhibits a well-defined oxidation peak at 1.2 V. The peak potential is 200 mV negative to that at p-MWCNT/DHP/TaE, suggesting that MWCNT/DHP/TaE has a much higher electrocatalytic activity to the oxidation of SV. Interestingly, MWCNT/DHP/TaE exhibited an increased oxidation current at the potential of 1.2 V than p-MWCNT/DHP/TaE. The lower oxidation overpotential and increased oxidation current than those of p-MWCNTs confirm that nitrogen-doped MWCNTs possess an excellent catalytic activity toward the oxidation of SV. This excellent catalytic activity can be used to detect the SV concentration at low potential with high sensitivity.

In addition, EIS was also employed to investigate the impedance changes of the electrode surfaces due to the nitrogen doping. Figure 10 shows the Nyquist plots of $K_3Fe(CN)_6/K_4Fe(CN)_6$ at the pristine MWCNT/TaE and the nitrogen-doped A-MWCNT/TaE. As it can be seen, the R_{ct} values for nitrogen-doped MWCNT-modified electrode (curve B) are somewhat smaller compared to those obtained on film consisting of pristine MWCNTs (curve A). The last finding confirms the important effect of nitrogen doping on electrocatalytic activity of carbon nanotubes. Namely, it is obvious that the barrier for electron transfer is significantly reduced on nitrogen-doped carbon nanotubes.

The density of A-CNTs may influence their inherent properties, such as electron transfer rate and electrocatalytic activity, and it may also influence the immobilization of biomolecule and the diffusion of substrate, which will finally influence the detecting performance of the biosensor modified with the ACNTs. The site density of the A-CNTs can be controlled by tuning the site density of Ni nanoparticles, which serve as catalysts [42]. In order to investigate the effect of CNTs density on sensing performance, low-density-aligned carbon nanotubes (LD-ACNTs) with a

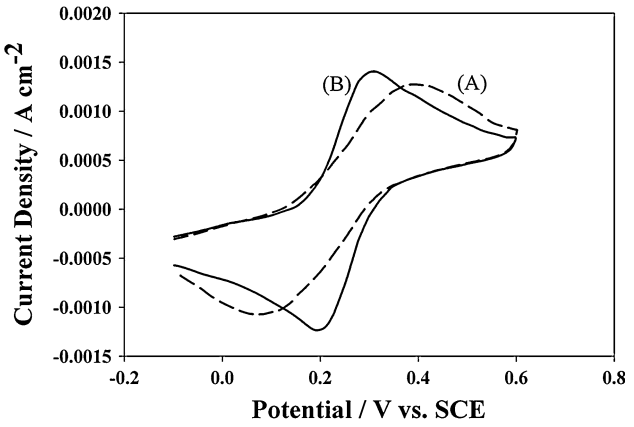

Fig. 11 Cyclic voltammograms of **a** HD-ACNTs/Ta electrode, **b** LD-ACNTs/Ta-modified electrode in 5.0 mM $K_4Fe(CN)_6/K_3Fe(CN)_6$, with scan rate of 20 mV s^{-1}

site density of 1×10^9 cm^{-2} and high-density-aligned carbon nanotubes (HD-ACNTs) with a site density of 1×10^{12} cm^{-2} were prepared by varying the thickness of Ni catalyst and were used to form ACNTs/Ta electrode. As a matter of fact, thicker nickel films higher up the density of the CNTs. It means thickness of the metallic film controls density and dimension of the metallic particles and, therefore, density and diameter of the CNTs. Thicker nickel films result in bigger nickel particles with higher density during CVD, leading to thicker CNTs of higher density, whereas thinner nickel films result in smaller nickel particles that are more sparsely distributed thereby producing thinner CNTs with lower density. If there is scarce amount of the chloride solution on the surface result in very thin nickel film, a sparse distribution of nickel particles forms and there are not enough particles to produce CNTs, and consequently there are voids in the film of CNTs and the CNTs formed are sparse. So, thin metallic film leads to fabrication of separated CNTs. However, CNTs growth hinders on the thick metallic film, because thick metallic films fail to separate into nanoparticles and are prone to sinter during CVD; so, enough nanoparticles to feed CNTs are not produced. Thus, appropriate film thickness can be defined by number of chloride-nickel film layers and its concentration.

The advantages of LD-ACNTs/TaE were demonstrated by comparing with HD-ACNTs/TaE in reversibility and effective surface area. Figure 11 shows the cyclic voltammograms of the electrodes modified with high (curve A) and low density (curve B) of ACNTs at scan rate of 20 mV s^{-1} in 5 mM $Fe(CN)_6^{4-/3-}$.The peak potential difference of the LD-ACNTs/TaE electrode is about 110 mV, which is much smaller than that of the HD-ACNTs/TaE electrode (300 mV). The peak potential difference between the anodic peak and cathodic peak can

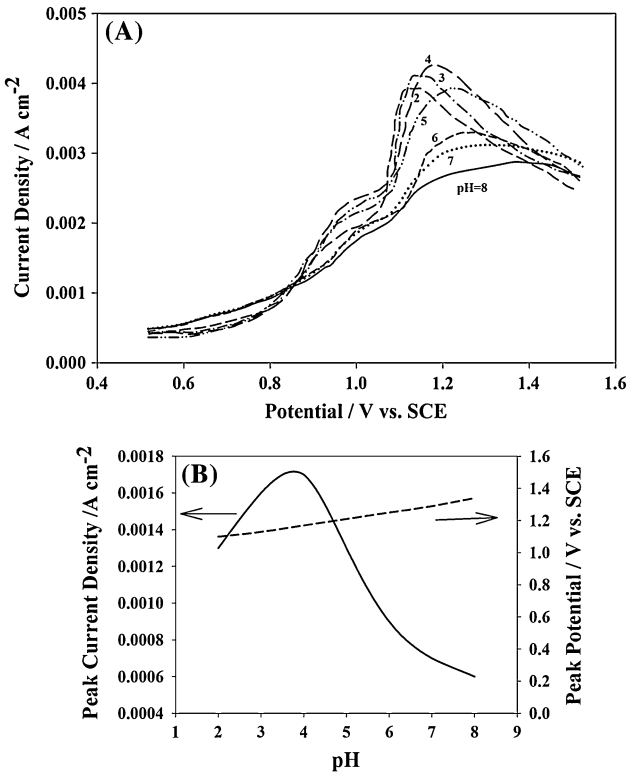

Fig. 12 **a** Differential pulse voltammograms of 1×10^{-6} M SV at different pH values. Supporting electrolyte: PBS (0.1 M, pH = 4); pulse amplitude = 50 mV; pulse width = 50 ms; pulse period = 0.2 s. **b** The effect of pH value on peak current density and potential of SV oxidation at A-MWCNTs/DHP/TaE

denote the reversibility of an electrode. The smaller the peak potential difference, the better the reversibility of the electrode. From the peak potential difference, it can be concluded that LD-ACNTs/TaE electrode has better reversibility than the HD-ACNTs/TaE electrode. So, the electron transfer rate on LD-ACNTs/TaE is larger than that on HD-ACNTs/TaE. Also, at LD-ACNTs/TaE, the redox probe reaction is significantly improved (curve B), reflected by the enlarged peak current and the negative shift of the redox peak potential in contrast to the HD-ACNTs/Ta electrode (curve A). The negative shift of the peak potential in addition to enhancement in peak current sharpness and amount at this modified electrode shows a strong catalytic function due to high electroactive surface areas. On the other hand, the spacing in the LD-ACNTs can make every nanotube work as an individual nanoelectrode [43], which is also contributive to the high sensitivity of the modified electrode to SV.

3.6 The effect of pH on the oxidation of SV at the A-MWCNT/DHP/TaE

As a rapid and powerful method, the DPV with the following optimized conditions was employed in the

determination of SV; pulse amplitude = 50 mV; pulse width = 50 ms; pulse period = 0.2. In order to find out the most suitable pH for supporting electrolyte to be employed in analytical determinations, pH dependency of peak current and peak potential were investigated over the pH range 2.0–8.0 using DPV technique (Fig. 12a). Due to higher sensitivity of the oxidation response of the SV at potential of 1.2 V, this peak has been considered for further investigations.

It was found that the peak current increased upon the decrease of pH value from 8.0 to 4.0, but later on, it decreased with the further reduction of pH to 2.0. The peak current reached a maximum value at pH 4.0. As is mentioned protons participated in SV oxidation; thus, the peak current decreased at pH higher than 7.0 in base solutions, and even it disappeared. The effect of pH on the oxidation peak potential is differently varied. Meanwhile, with the increase of pH value from 2.0 to 8.0, the peak potential shifted toward positive and exhibited a linear relationship, which has a slope of 0.0395 (Fig. 12b). The equation relating E_p (in V vs. SCE) with pH, over the pH range of 2.0–8.0 (Fig. 12b), can be shown by the following equation:

$$E_{p,a}(\mathrm{V}) = +1.0163 + 0.0395\ \mathrm{pH}\ \left(R^2 = 0.994\right). \quad (1)$$

The abnormal variation of the peak potential with pH might be arisen from the coexistence of SV and its hydrolyzed product, since SV might be hydrolyzed into SVA at high pH values [44]. Considering both the peak current and the peak shape, pH = 4.0 was chosen as the optimized pH of supporting electrolyte [PBS (0.1 M)] in all voltammetric determinations.

3.7 Influence of scan rate on SV oxidation

The effects of different scan rates on the oxidation of SV at the A-MWCNT/DHP/TaE in 1.0 μM SV in PBS using CV are shown in Fig. 13a. As shown in the Fig. 13b, the peak current increased with the increase of the scan rate, and a good linearity between scan rate and peak current density could be obtained within the range of 10–100 mV s^{-1}. This indicates that the electrochemical kinetics is controlled by the adsorption of SV which represents an adsorption-controlled process. This result was in accordance with the disappearance of the oxidation peak in the second cycle of the successive voltammograms. The regression equation for this relationship is:

$$i_{p,a} = 1 \times 10^{-4} + 6 \times 10^{-6} v \quad \left(R^2 = 0.998,\ i_{p,a}:\ \mathrm{A\,cm^{-2}},\ v:\ \mathrm{mV\,s^{-1}}\right). \quad (2)$$

The effect of scan rate on oxidation peak potential was also studied. The peak potential shifted to positive values with increasing scan rates. In the range of 10–100 mV s^{-1}, the peak potential has a relationship with scan rate (v):

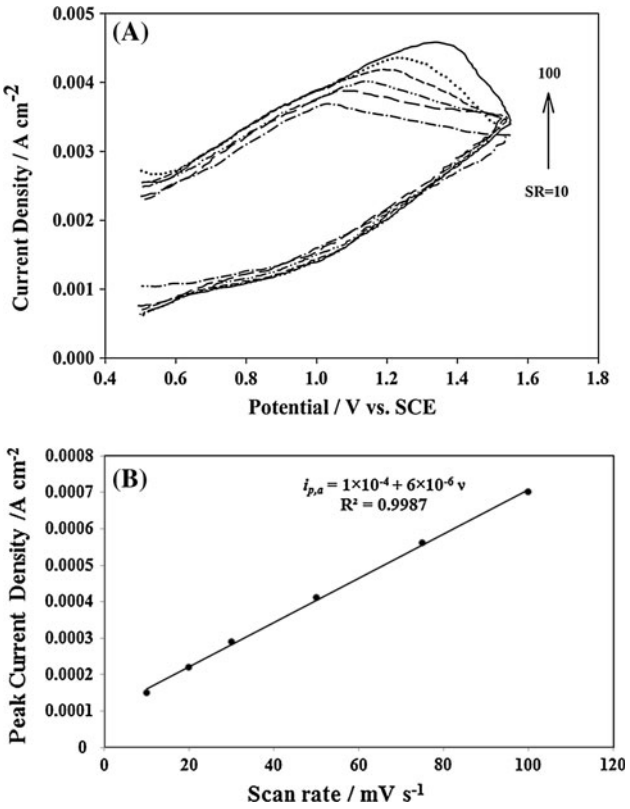

Fig. 13 **a** CVs of A-MWCNTs/DHP/Ta electrode at different scan rates (10–100 mV s^{-1}) in PBS (0.1 M, pH = 4). **b** The plot of oxidation peak current density with scan rate

$$E_p = 0.178 + 0.27 \log v \ \left(R^2 = 0.996,\ E_p:\ \mathrm{V},\ v:\ \mathrm{V\,s^{-1}}\right). \quad (3)$$

According to Zhang and Wang [45], the relationship between the peak potential and the scan rate for adsorbed species in the completely irreversible electrochemical process can be expressed as

$$E_p = (1/2)\, b \log v + a, \quad (4)$$

where $b = 2.303RT/(1 - \alpha)n_\alpha F$, a value of 0.33 was estimated for the term $(1 - \alpha)n_\alpha$. By considering a value of 0.66 for the α, which indicates that the activation free energy curve is not symmetric in such an irreversible oxidation process, one electron was involved in the rate-determining step for SV oxidation.

3.8 Influence of accumulation time on the oxidation of SV

The influence of the accumulation time on the oxidation current of SV was investigated via DPV. It has been mentioned that the oxidation of SV at the A-MWCNTs/DHP/TaE was controlled by the adsorption process and SV might be accumulated on the electrode surface through the

hydrophobic interaction between SV and the DHP layer. Figure 14a shows the dependence of the oxidation peak current density on the accumulation time. In the range of 1–4 min of accumulation time, the oxidation peak current almost exhibited a linear relationship with the accumulation time (Fig. 14b). At 5 min, the oxidation peak current tended to remain stable, indicating a saturated adsorption of SV at the electrode surface. However, by further increasing the accumulation time, the response current decreased. Longer accumulation time resulted in the separation of DHP from the MWCNT surface by stirring, thus SV would not be adsorbed to the DHP layer, and, therefore, the oxidation peak current of SV would be decreased (Fig. 14b). This supported the conclusion that SV was adsorbed at the A-MWCNTs/DHP/TaE via hydrophobic interaction. Therefore, time of 4 min was chosen as optimum accumulation time in the following experiments.

3.9 Linear response of the A-MWCNTs/DHP/TaE and calibration curve

The DPV responses of the A-CNT electrode to the sequent addition of SV were investigated. Figure 15 shows the DPV response of SV at the A-MWCNTs/DHP/TaE in PBS (pH = 4.0) with concentration. The A-MWCNTs/DHP/TaE responds rapidly to the changes in SV concentration (Fig. 15). The inset of Fig. 15 shows the calibration curve of the peak current density versus the concentration of SV. In fact, the DPV current response is linearly dependent on the concentration of SV in a wide range of 0.01–1.0 μM with a slope of 0.001 A cm^{-2} μM^{-1} (the sensitivity of the electrode) and the correlation coefficient of 0.9994. This sensitivity of the used sensor is substantially higher than that of the previously reported SV sensor using entangled MWCNTs-DHP/GCE electrode, about 1,000-fold, and this high sensitivity is accompanied with a low noise level despite the large voltammetric background current [46]. Also, the detection limit is 0.01 nM with a signal-to-noise of 3, which is 1,000-fold lower than the previously reported sensors using entangled MWCNT-DHP/GCE electrodes for selective detection of SV (0.05 μM) [46]. This is owing to the alignment, regular pore structures, and conductive paths of MWCNT electrode which facilitates high catalytic activity and electron transfer toward SV.

3.10 Reproducibility and long-term stability of the A-MWCNTs/DHP/TaE

The reproducibility, repeatability, and the long-term stability of the response are important parameters for the evaluation of the performance of a sensor. The reproducibility of the A-MWCNT/DHP/TaE for the determination of SV was investigated. In order to study the reproducibility of the electrode preparation procedure, six modified electrodes based on the same fabrication procedure were

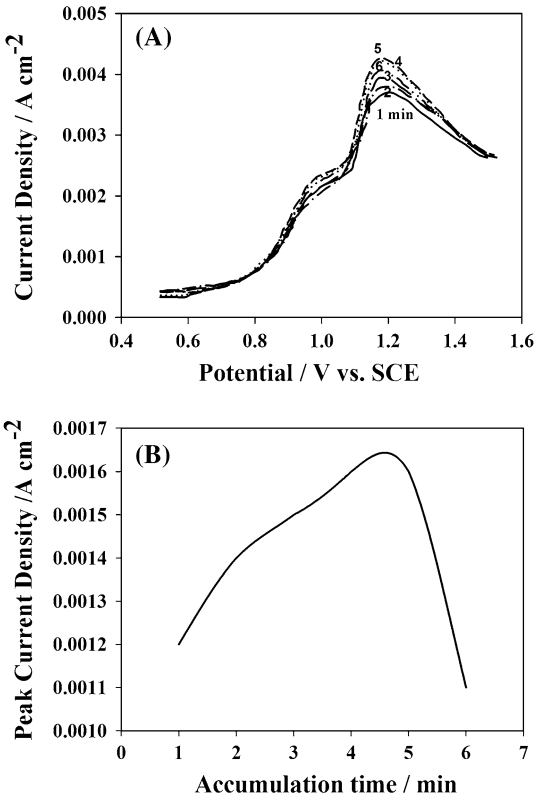

Fig. 14 **a** DPV of 1×10^{-6} M SV in PBS (0.1 M, pH = 4) at A-MWCNTs/DHP/TaE with different accumulation times. Scan rate = 20 mV s^{-1}. **b** The relationship between oxidation peak current density and accumulation time

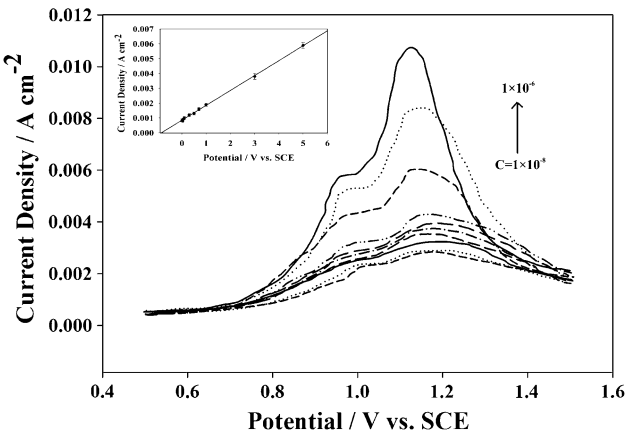

Fig. 15 Differential pulse voltammograms of A-MWCNTs/DHP/TaE in 0.10 M PBS solution with various concentrations of SV, from bottom to top in the range of between 1×10^{-8} and 1×10^{-6} M. Pulse amplitude = 50 mV; pulse width = 50 ms; pulse period = 0.2 s. *Inset* shows plot of peak current density versus SV concentration

prepared and used for the determination of 1.0 μM SV in PBS (pH = 4.0). The RSD for the peak current determinations with six prepared electrodes on 1.0 μM SV was calculated to be 2.4 % (for averages of six determinations on each electrode). This demonstrates that the prepared electrode was highly reproducible. In order to investigate the repeatability of the modified electrode, SV was repeatedly determined 6 times in a fixed SV concentration of 1.0 μM with the same modified electrode, and the RSD for the peak currents in DPVs based on six replicates was 1.8 %. This indicates the excellent repeatability of the response of the modified electrode. Also, on using the A-MWCNT/DHP/TaE daily and storing under ambient conditions over a period of 2 weeks, the electrode retained 96.4 % of its initial peak current response for a SV concentration of 1.0 μM, which shows long-term stability of the film modifier on the surface of modified electrode. The results indicate that the modified electrode has an excellent repeatability and reproducibility in both preparation procedure and voltammetric determinations with good long-term stability.

3.11 Anti-interference properties of the A-MWCNTs/DHP/TaE toward SV Sensing

It is critical to establish analytical approach to determine SV in the presence of AA and other acids like UA. Figure 16a shows DPV responses of 10.0 μM SV, AA, and UA in 0.1 M PBS separately, and Fig. 16b shows responses of 10.0 μM SV containing 100.0 μM AA and 100.0 μM UA in 0.1 M PBS at the A-MWCNTs/DHP/TaE. In the absence of SV, DPV of AA and UA presented two anodic oxidation peaks at 0.09 and 0.4 V, which are corresponding to AA and UA, respectively (Fig. 16a).With increasing 10.0 μM SV, it can be seen that SV exhibits excellent DPV response with the other two ingredients remaining unchanged (Fig. 16b). The separations among the three potential peaks are enough for the determination of the three species. It proves that the responses to AA, SV, and UA at the A-MWCNTs/DHP/TaE are relatively independent. Thus, 100.0 μM AA and UA did not interfere in SV detection and do not have any serious effects on the electrochemical response of the modified electrode. These results show that the simultaneous determination of the three species, with well-separated three anodic peaks, could be possible at the A-MWCNT/DHP/TaE. Some other statins with similar structures to SV, such as lovastatin, seriously interfered in the SV determination. However, the contents of these statins in SV tablets were very low, and their interferences were small.

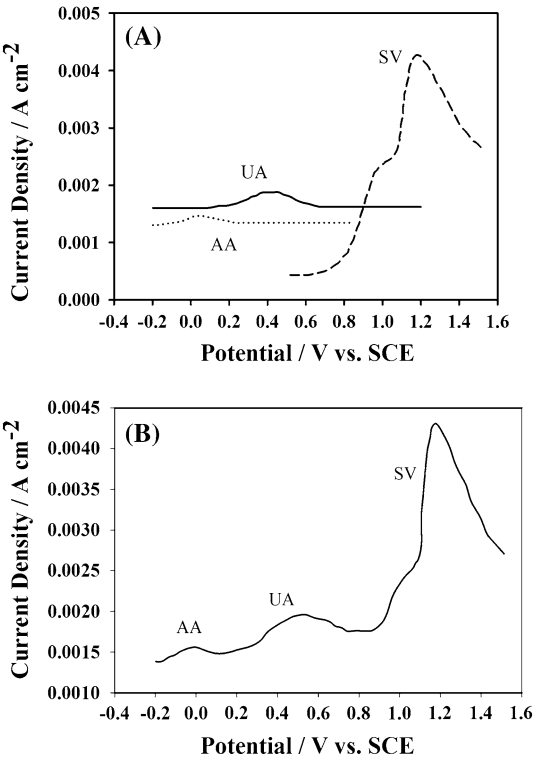

Fig. 16 Differential pulse voltammograms of A-MWCNTs/DHP/Ta electrode in solutions containing **a** 1×10^{-5} M SV, AA, and UA in 0.1 M PBS separately and **b** 1×10^{-5} M SV, 1×10^{-4} M AA, and 1×10^{-4} M UA together in 0.1 M PBS. Pulse amplitude = 50 mV; pulse width = 50 ms; pulse period = 0.2 s

3.12 Analytical application in real samples; determination of SV in pharmaceutical dosage form

To assess the applicability of the proposed method, the A-MWCNT/DHP/TaE was used for determination of the content of SV in "simvastatin" tablets as a real pharmaceutical sample using the standard addition method. According to the results of the standard addition–calibration plot, it is observed that tablet matrix does not have any interference effect on the electrochemical analysis of SV, although the accuracy was calculated on the recovery of known amounts of the standard SV solution spiked in tablet solution. Spiked samples were prepared at five levels. The results are demonstrated in Table 2, and the recoveries were in the range from 99.10 to 104.85 %, suggesting the successive applicability of the proposed strategy for the clinical applications. Using this standard addition method, the SV content was obtained to be 19.30 mg with a RSD of 3.7 % ($n = 4$) per tablet, which is very close to the labeled amount 20.0 mg and indicating adequate precision and accuracy of the proposed method.

Table 2 Results of the recovery analysis of SV spiked in tablet samples

No.	Spiked (μM)	Expected (μM)	Found[a] (μM)	Recovery (%)
1	0	0.3	0.29	–
2	0.2	0.5	0.51	102.40
3	0.4	0.7	0.73	104.85
4	0.7	1	1.02	102.20
5	2.7	3	2.97	99.10
6	4.7	5	5.05	101.14

[a] Average of four replicate measurements (rounded)

4 Conclusion

In summary, we demonstrated herein the first usage of highly oriented MWCNTs in a sensor configuration for investigating the electrochemical oxidation and determination of SV. The oriented nanotube forest on the Ta substrate electrically behaves similar to a metal, conducts electron fast and easily, and the preparation of these prototype well-aligned MWCNT sensors is effective. CVs of SV demonstrate that the oxidation of SV at A-MWCNTs/DHP/TaE showed a greatly enlarged current response which is over 200-fold higher than the previously reported value at entangled MWCNTs-DHP/GCE electrode. In the sensor proposed here, the current response is linearly dependent on the concentration of SV between a wide detection range of 100.0 and 1.0 μM with a slope of 0.001 A cm^{-2} μM^{-1}. Also, the detection limit is 0.01 nM with a signal-to-noise of 3, which is 1,000-fold lower than the previously reported sensor fabricated using entangled MWCNT electrode. This improved characteristic is owing to the perfect alignment of MWCNT electrode and its large active surface area which facilitates high catalytic activity toward SV. When these superior performance characteristics are combined with the ease of fabrication, excellent reproducibility and excellent specificity to SV in the presence of common interferes, the A-MWCNT/DHP-modified electrode becomes a potential candidate for routine SV analysis and highly promising as an SV sensor.

References

1. Myant NB (1981) The biology of cholesterol and related steroids. Willium Heinemann Medical Books Ltd., London
2. Fredrickson DS, Levy RI (1972) In: Fredrickson DD, Wyngarden JB (eds) The metabolic basis of inherited disease, McGraw-Hill, New York, pp 545–546
3. Hoffman WF, Alberts AW, Anderson PS, Chen JS, Amith RL, Willard AK (1986) 3-Hydroxy-3-methylglutaryl-coenzyme A reductase inhibitors. 4. Side chain ester derivatives of mevinolin. J Med Chem 29:849–852
4. Carlucci G, Mazzeo P, Biordi L, Bologna M (1992) Simultaneous determination of simvastatin and its hydroxy acid form in human plasma by high performance liquid chromatography with UV detection. Pharm J Biomed Anal 10:693–697
5. Jemal M, Ouyang Z, Powell ML (2000) Direct-injection LC–MS–MS method for high-throughput simultaneous quantitation of simvastatin and simvastatin acid in human plasma. J Pharm Biomed Anal 23:323–340
6. Wang L, Asgharnejad M (2000) Second-derivative UV spectrometric determination of simvastatin in its tablet dosage form. J Pharm Biomed Anal 21:1243–1248
7. Gaichore RR, Srivastava AK (2012) Multiwalled carbon nanotube-4-*tert*-butyl calix[6]arene composite electrochemical sensor for clenbuterol hydrochloride determination by means of differential pulse adsorptive stripping voltammetry. J Appl Electrochem 42:979–987
8. Fei J, WenX Yi L, Ge F, Zhang Y, Huang M, Chen X (2008) Electrochemical determination diethylstilbestrol by a single-walled carbon nanotube/platinum nanoparticle composite film electrode. J Appl Elechtrochem 38:1527–1533
9. Iijima S (1991) Helical microtubules of graphitic carbon. Nature 354:56–58
10. Peng H, Sun X, Cai F, Chen X, Zhu Y, Liao G, Chen D, Li Q, Lu Y, Zhu Y, Jia Q (2009) Electrochromatic carbon nanotube/polydiacetylene nanocomposite fibres. Nature Nanotechnol 4:738–741
11. Sun X, Wang W, Qiu L, Guo W, Yu Y, Peng H (2012) Unusual reversible photomechanical actuation in polymer/nanotube composites. Angew Chem Int Ed 51:1–6
12. Aravinda LS, Nagaraja KK, Nagaraja HS, Udaya Bhat K, Ramachandra BhatB B (2013) Magnetron sputtered MoO_3/carbon nanotube composite electrodes for electrochemical supercapacitor. Electrochim Acta 95:119–124
13. Manjunatha R, Nagaraju DH, Suresh GS, Melo JS, Souza SFD, Venkatesha TV (2011) Direct electrochemistry of cholesterol oxidase on MWCNTs. J Electroanal Chem 651:24–29
14. Salinas-Torres D, Huerta F, Montilla F, Morallón E (2011) Study of electroactive and electrocatalytic electrodes surfaces of single walled carbon nanotube modified. Electrochim Acta 56:2464–2470
15. Barisci JN, Wallace GG, Baughman RH (2000) Electrochemical studies of single wall carbon nanotube in aqueous solutions. J Electroanal Chem 488:92–98
16. Sun X, Chen T, Yang Z, Peng A (2013) The alignment of carbon nanotubes: an effective route to extend their excellent properties to macroscopic scale. Acc Chem Res 46:539–549
17. Sun X, Zhang Z, Lu X, Guan G, Li H, Peng H (2013) Electric current test paper based on conjugated polymers and aligned carbon nanotubes. Angew Chem Int Ed 52:7776–7780
18. HondaY HaramotoT, Takeshige M, Shiozaki H, Kitamura T, Ishikawa M (2007) Aligned MWCNT sheet electrodes prepared by transfer methodology providing high-power capacitor performance. Electrochem Solid-State Lett 10:106–110
19. Zhang WD, Wen Y, Lin SM, Tjiu WC, Xu GQ, Gan LM (2000) Synthesis of vertically aligned carbon nanotubes on metal deposited quartz plates. Carbon 40:1981–1989
20. Talapatra S, Kar S, Pal SK, Vajtai R, Ci L, Victor P (2006) Growth of aligned nanotubes on bulk metals. Nat Nanotechnol 1:112–116
21. Hiraoka T, Yamada T, Hata K, Futaba DN, Kurachi H, Uemura S (2006) Synthesis of single- and double-walled carbon nanotube forests on conducting metal foils. J Am Chem Soc 128:13338–13339
22. Farmer JC, Fix DV, Mack GV, Pekala RW, Poco JF (1996) Capacitive deionization of NaCl and $NaNO_3$ solutions with carbon aerogel electrodes. J Electrochem Soc 143:159–169

23. Fraczek-Szczypta A, Menaszek E, Syeda TB, Misra A, Alavijeh M, Adu J, Blazewicz S (2012) Effect of MWCNT surface and chemical modification on in vitro cellular response. J Nanopart Res 14:1181–1195
24. Mawhinney DB, Naumenko V, Kuznetsova A, Yates JT (2000) Infrared spectral evidence for the etching of carbon nanotubes: ozone oxidation at 298 K. J Am Chem Soc 122:2383–2384
25. Goyanes S, Rubiolo GR, Salazar A, Jimeno A, Corcuera MA, Mondragon I (2007) Carboxylation treatment of multiwalled carbon nanotubes monitored by infrared and ultraviolet spectroscopies and scanning probe microscopy. Diam Relat Mater 16:412–417
26. Sotiropoulou S, Chaniotakis NA (2003) Carbon nanotube array-based biosensor. Anal Bioanal Chem 375:103–105
27. Britto PJ, Santhanam KSV, Rubio A, Alonso JA, Ajayan PM (1999) Improved charge transfer at carbon nanotube electrodes. Adv Mater 11:154–157
28. Lee YT, Kim NS, Park J (2003) Temperature-dependent growth of carbon nanotubes by pyrolysis of ferrocene and acetylene in the range between 700 and 1000 °C. Chem Phys Lett 372:853–859
29. Ni L, Kuroda K, Zhou LP, Kizuka T, Ohta K, Matsuishi K (2006) Kinetic study of carbon nanotube synthesis over Mo/Co/MgO catalysts. Carbon 44:2265–2272
30. Tuinstra F, Koenig JL (1970) Raman spectrum of graphite. J Chem Phys 53:1126–1130
31. Chiu PW, Duesberg GS, Dettlaff-Weglikowska U, Roth S (2002) Interconnection of carbon nanotubes by chemical functionalization. App Phys Lett 80:3811–3813
32. Liu H, Zhang Y, Li R, Sun X, De′silets S, Abou-Rachid H (2010) Structural and morphological control, nitrogen incorporation and stability of aligned nitrogen-doped carbon nanotubes. Carbon 48:1498–1507
33. Zhao M, Xia Y, Ma Y, Ying M, Liu X, Mei L (2002) Exohedral and endohedral adsorption of nitrogen on the sidewall of single-walled carbon nanotubes. Phys Rev B 66:155403
34. Reyes–Reyes M, Grobert N, Kamalakaran R, Seeger T, Golberg E, Ruhle M (2004) Efficient encapsulation of gaseous nitrogen inside carbon nanotubes with bamboo-like structure using aerosol thermolysis. Chem Phys Lett 396:167–173
35. Choi HC, Baes SY, Park J, Seo K, Kim C, Kim B (2004) Experimental and theoretical studies on the structure of N-doped carbon nanotubes: possibility of intercalated molecular N_2. Appl Phys Lett 85(23):5742–5744
36. Kwon JY, Kim HD (2005) Preparation and properties of acid treated multiwalled carbon nanotube/waterborne polyurethane nanocomposites. J Appl Polym Sci 96:595–604
37. Wang EG (2006) Nitrogen-induced carbon nanobells and their properties. J Mater Res 21(11):2767–2773
38. Kong J, Franklin NR, Zhou C, Chapline MG, Peng S, Cho K, Dai H (2000) Nanotube molecular wires as chemical sensors. Science 287:622–625
39. Friedrich J, Zuzek M, Bencina M, Cimerman A, Strancar A, Rades I (1995) High-performance liquid chromatographic analysis of mevinolin as mevinolinic acid in fermentation broths. J Chromatogr 204:363–367
40. Nevcidomskyy AH, Csanyi G, Payne C (2003) Chemically active substitutional nitrogen impurity in carbon nanotubes. Phys Rev Lett 91(10):105502
41. Katz E, Willner I (2004) Biomolecule-functionalized carbon nanotubes: applications in nanobioelectronics. Chem Phys Chem 5:1084–1104
42. Yue B, Ma YW, Tao HS, Yu LS, Jian GQ, Wang XZ, Wang XS, Lu YN, Hu Z (2008) CNx nanotubes as catalyst support to immobilize platinum nanoparticles for methanol oxidation. J Mater Chem 18:1747–1750
43. Tu Y, Huang ZP, Wang DZ, Wen JG, Ren ZF (2002) Growth of aligned carbon nanotubes with controlled site density. Appl Phys Lett 80:4018–4020
44. Morf WE, de Rooij NF (1997) Performance of amperometric sensors based on multiple microelectrode arrays. Sens Actuators B44:538–541
45. Zhang Z, Wang E (2000) Electrochemical principles and methods. Science Press, Beijing, p 242
46. Zhang H, Hu C, Wu S, Hu S (2005) Enhanced oxidation of simvastatin at a multi-walled carbon nanotubes—dihexadecyl hydrogen phosphate composite modified glassy carbon electrode and the application in deter—mining simvastatin in pharmaceutical dosage forms. Electroanalysis 17:749–754